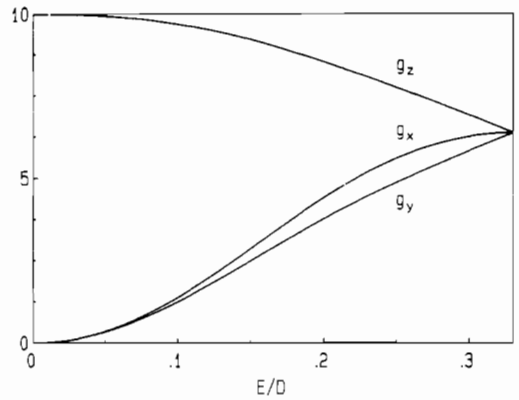

Figure 7. Variation of the principal values of the **g** tensors for the ground state of a $S = {}^9/_2$ system as a function of the E/D parameter.

$(CTH)_2(DHBQ)(ClO_4)_3$. In fact this compound has a ground $S = {}^5/_2$ state and one isotropic g value at $g \approx 4$. It is well-known from the EPR spectra of high-spin iron(III) complexes that when the metal ion is in a completely rhombic coordination environment, only the transitions within the middle Kramers doublet of the zero-field-split $S = {}^5/_2$ manifold are observed:[37] these are isotropic with $g = 4.3$. We assume that the origin of the EPR spectrum of $Cr_2(CTH)_2(DHBQ)(ClO_4)_3$ is the same, with the small reduction in the g value determined by the fact that the chromium ion has a g value that is slightly lower than 2.

If this interpretation is correct, it is tempting to assume that also for the $S = {}^9/_2$ state the origin of the spectra is similar; i.e., they are due to transitions within a Kramers doublet in rhombic symmetry. By using the spin Hamiltonian approach, it is easy to show that an isotropic g feature arising from the middle Kramers doublet is not peculiar to $S = {}^5/_2$ states, but it can be extended to all the $S = (4n + 1)/2$ states that split into an odd number of Kramers doublets. In the limit of maximum rhombic splitting, which corresponds to $E/D = \pm{}^1/_3$, the Kramers doublets of $S = {}^9/_2$ have energies $\pm(11.7D + 1.8E)$, $\pm(4.6D + 1.2E)$, and 0 and the central Kramers doublet has an isotropic g value of $35g_s/11$, where g_s is the value for the spin multiplet. For $g_s = 2$, g is 6.3. For the interest of researchers who may stumble on high-spin states, the isotropic g value for $S = {}^{13}/_2$ is 8.3, for $S = {}^{17}/_2$ is 10.2, and for $S = {}^{21}/_2$ it is 12.0. These values are calculated in the assumption $g_s = 2$.

When the E/D ratio decreases from the limit value of ${}^1/_3$ for $S = {}^9/_2$, two g values move toward zero, while the third tends to 10 at $E/D = 0$. The dependence of the g values on the E/D ratio is shown in Figure 7.

Assuming that the EPR spectra of $Fe_2(CTH)_2(DHBQ)(ClO_4)_3$ are given by transitions within the middle doublet, they can be fitted to the polycrystalline powder spectrum of an effective $S = {}^1/_2$ with g values $g_1 = 5.5$, $g_2 = 5.0$, and $g_3 = 7.3$. These values show that the splitting of the $S = {}^9/_2$ manifold is not completely rhombic, suggesting $E/D = 0.28$.

Conclusion

The present results have shown that the radical species $DHBQ^{3-}$ can be stabilized with trivalent cations, such as iron(III) and chromium(III). $DHBQ^{3-}$ behaves essentially as an innocent ligand, which can yield reasonably strong antiferromagnetic coupling with the metal ions but smaller than that of simple *o*-semiquinones. It is hoped that by using this kind of ligands it is possible to build molecular based ferromagnets.

Acknowledgment. The financial support of the CNR of the Progetto Finalizzato "Materiali Speciali per Tecnologie Avanzate" and of the MURST is gratefully acknowledged.

(37) Lang, G.; Aasa, R.; Garbett, K.; Williams, R. J. P. *J. Chem. Phys.* **1971**, *55*, 4539.

Contribution from the Chemistry Department, Kuwait University, Box 5969, 13060 Safat, Kuwait

Quasirelativistic Effects in the Electronic Structure of the Thiomolybdate and Thiotungstate Complexes of Nickel, Palladium, and Platinum

B. D. El-Issa*,† and M. M. Zeedan

Received May 14, 1990

In this paper, we present a comparative study of the thiomolybdate and the thiotungstate complexes of the formula $[M'(MS_4)_2]^{2-}$ (M' = Ni, Pd, Pt; M = Mo, W). The electronic structure and the bonding properties of these complexes are discussed by using the quasirelativistic multiple scattering $X\alpha$ method. We have repeated the calculations for the $[Pt(WS_4)_2]^{2-}$ complex ion without incorporating the mass velocity and the Darwin corrections around the Pt sphere, and certain conclusions are obtained regarding the relativistic and the nonrelativistic effects on these complex ions. Transition and ionization energies are also discussed.

Introduction

The thioanions $[MS_4]^{2-}$ (M = Mo, W), which act as bidentate chelating ligands with transition metals, have been of great interest for many years.[1,2] They have a bioinorganic significance, particularly in the ligand-exchange processes in aqueous solutions.[3,4] The thiomolybdate complex ion plays an important role in the nitrogenase problem and Cu-Mo antagonism.[5] These anions have been studied spectroscopically[6-12] and theoretically.[13-15] Various theoretical calculations have been conducted on the $[MoS_4]^{2-}$ complex ion,[15] and most of these studies have indicated that the HOMO is essentially of S(p) character. This orbital can act as a donor in complexes that contain a transition metal, as may be verified in Figure 1, which is a correlation diagram for $[MoS_4]^{2-}$ in a tetrahedral environment. Tetrathiomolybdates and tetrathiotungstates can produce multimetal complexes of the type

† Present address: Chemistry Department, University of Jordan, Amman, Jordan.

(1) Mccleverty, J. A. *Prog. Inorg. Chem.* **1968**, *10*, 49-221.
(2) Eisenberg, R. *Prog. Inorg. Chem.* **1970**, *12*, 295-369.
(3) Diemann, E.; Müller, A. *Coord. Chem. Rev.* **1973**, *10*, 79-122.
(4) Volger, A.; Kunkely, H. *Inorg. Chem.* **1988**, *27*, 504-507.
(5) Müller, A.; Diemann, E.; Jostes, R.; Bögge, H. *Angew. Chem., Int. Ed. Engl.* **1981**, *20*, 934-955.
(6) Barth, J. A.; Leipzig, *Z. Anorg. Allg. Chem.* **1972**, *391*, 38-53.
(7) Bartecki, A.; Dembicka, D. *Inorg. Chem. Acta* **1973**, *7*, 610-612.
(8) Schmidt, K. H.; Müller, A. *Coord. Chem. Rev.* **1974**, *14*, 115-179.
(9) Petit, R. H.; Briat, B.; Müller, A.; Diemann, E. *Mol. Phys.* **1974**, *27*, 1373-1384.
(10) Clark, R. J. H.; Dines, T. J.; Wolf, M. L. *J. Chem. Soc., Faraday Trans. 2* **1982**, *78*, 679-688.
(11) Clark, R. J. H.; Dines, T. J.; Proud, G. P. *J. Chem. Soc., Dalton Trans.* **1983**, No. 9, 2019-2024.
(12) Liang, K. S.; Bernholc, J.; Pan, W.-H.; Hughes, G. J.; Stiefel, E. I. *Inorg. Chem.* **1987**, *26*, 1422-1425.

0020-1669/91/1330-2594$02.50/0

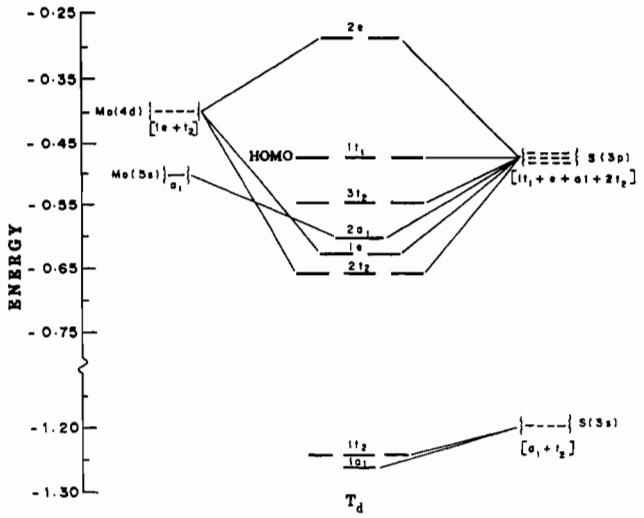

Figure 1. Interaction diagram that shows the MS–Xα orbital energies (in rydbergs) for $[MoS_4]^{2-}$ in a tetrahedral environment.

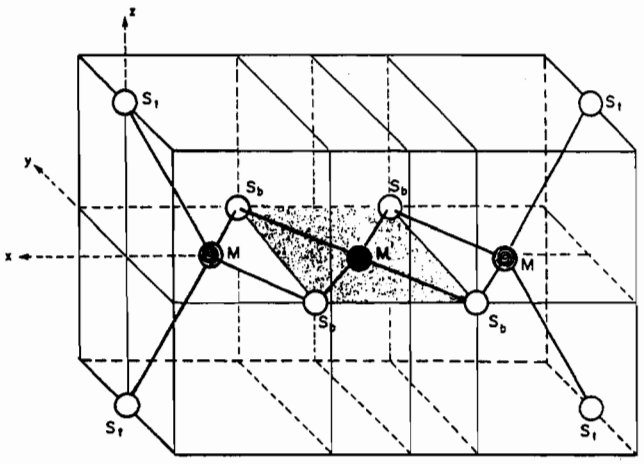

Figure 2. Structure of the thiomolybdate and thiotungstate complexes of the type $[M'(MS_4)_2]^{2-}$ (M' = Ni, Pd, Pt; M = Mo, W) under the D_{2h} environment.

$[M'(MS_4)_2]^{2-}$ (M' = Ni, Pd, Pt; M = Mo, W). Salts of $[Ni(MoS_4)_2]^{2-}$, $[Ni(WS_4)_2]^{2-}$, and $[Pt(MoS_4)_2]^{2-}$ were first prepared by Müller and co-workers[16-18] and later by Callahan and Piliero, who reported the synthetic preparation of $[Pd(MoS_4)_2]^{2-}$, $[Pd(WS_4)_2]^{2-}$, and $[Pt(WS_4)_2]^{2-}$ complexes.[19,20] On the basis of X-ray data for the $[Ni(MoS_4)_2]^{2-}$ complex ion,[21] it was suggested that the structure of these ions possesses D_{2h} symmetry with a square-planar coordination around the central metal and a tetrahedral coordination around the Mo and W centers (Figure 2). Salts of these ions were determined to be diamagnetic in solution and in their solid states.[20] It has also been shown by IR spectral measurements that the $[^{56}Ni(MoS_4)_2]^{2-}$ ion and its ^{62}Ni and ^{100}Mo analogues[22] exhibit a strong bond between the Ni(II) and the $[MoS_4]^{2-}$ ligands and that the structure does indeed possess D_{2h} symmetry. This is similar to other results obtained by infrared spectroscopy that suggested a strong ligand/metal interaction.[8]

Electrochemical studies reported by Callahan and Piliero[19,20] indicate that these complexes exhibit reversible electrochemical reduction processes. These results were also shown to be in agreement with the decreased separation of the a_g (LUMO) and the b_{1g} (HOMO) orbitals as the mass of the central metal increased.

On the basis of EH–SCCMO calculations on $[Ni(MS_4)_2]^{2-}$,[5] a strong π bond was determined to exist between the d_{xz} and d_{yz} orbitals of the Ni center and the ligand orbitals. Another bond was also determined to occur between the Ni atom and the two opposite S bridging atoms (S_b) of the two thiomolybdate ligands. In the case of the trimetallic complex ions $[M'(MS_4)_2]^{2-}$, the 3p nonbonding occupied ligand orbitals of sulfur were found to shift to a higher energy. Interaction between the M' center and/or the sulfur moieties was found to be of a σ nature.[5] Theoretical calculations on the $[Ni(MoS_4)]^{2-}$ complex ion suggest that the LUMO is of A_g symmetry, which is composed predominantly of the $Mo(d_{z^2})$ and $Mo(d_{x^2-y^2})$ bases.[23]

The Raman and resonance Raman studies that were reported by Clark and Walton[24] imply that all six complexes show electron delocalization in the excited state. A higher delocalization for the thiotungstate was observed in a manner similar to that of the thiomolybdate. This has been explained by the greater region of space that the 5d orbital of the W center occupies compared to that of the 4d orbital of Mo. The electronic spectra of these complexes were thought to constitute mainly charge-transfer bands that involve the central metal and the bridging sulfurs. The lowest energy transition band that was related to the $^1T_2 \leftarrow {}^1A_1$ transition of the $[MS_4]^{2-}$ ion was measured at 21 250 and 25 000 cm^{-1} for the Mo and W species, respectively. This band was observed to be split into two nearly equivalent components for the $[Ni(WS_4)_2]^{2-}$ and $[Pd(WS_4)_2]^{2-}$ complex ions, but for $[Pt(WS_4)_2]^{2-}$ it was determined to be shifted to a lower wavenumber. Similar absorption bands in the thiomolybdate complexes were reported not to be shifted, except for the $[Ni(MoS_4)_2]^{2-}$ case in which a shift to a lower wavenumber was observed.

A recent SCF–Xα calculation on the $[W_3S_8]^{2-}$ complex ion has been reported by Makhyoun[25] in which the bridging sulfur (S_b) moieties were determined to carry less negative charge than the corresponding terminal ones (S_t). As a result, the MO's of predominantly $S_b(3s)$ and $S_b(3p)$ bases were reported to be more stable than the analogous MO's of the terminal sulfurs. The nonbonding $8a_g$ orbital of this complex was reported to be principally composed of $d_{x^2-y^2}$ character of the central W, and the stability of the $7a_g$ orbital had been reported to be due to the σ-bonding interaction between the d_{z^2} components of the central (W_c) and the terminal (W_t) tungsten atoms.

Method

Spin-restricted scattered-wave Xα theory, originally descibed by Slater[26,27] and Johnson,[28,29] was used in this study to calculate ground-state electronic structures for the series of complex ions $[M'(MS_4)_2]^{2-}$ (M' = Ni, Pd, Pt; M = Mo, W). The parameters used in the calculations are summarized in Table I. Since the complexes under study are charged, a Watson sphere[30] with a charge of +2 and a radius slightly greater than that of the outer sphere was made to surround the clusters. Spherical harmonics up to a maximum angular momentum quantum number were

(13) Onopko, D. E.; Titov, S. A. *Opt. Spektrosk.* **1979**, *47*, 185–188.
(14) Bernholc, J.; Stiefel, E. I. *Inorg. Chem.* **1985**, *24*, 1323–1330.
(15) El.Issa, B. D.; Ali, A. A. M.; Zanati, H. *Inorg. Chem.* **1989**, *28*, 3297–3305.
(16) Müller, A.; Diemann, E. *J. Chem. Soc., Chem. Commun.* **1971**, No. 1, 65.
(17) Müller, A.; Ahlbor, E.; Heinsen, H.-H. *Z. Anorg. Allg. Chem.* **1971**, *386*, 102–106.
(18) Müller, A.; Chakrovorti, M. C.; Dornfield, H. *Z. Naturforsch.* **1975**, *B30*, 162–164.
(19) Callahan, K. P.; Piliero, P. A. *J. Chem. Soc., Chem. Commun.* **1979**, No. 1, 13–14.
(20) Callahan, K. P.; Piliero, P. A. *Inorg. Chem.* **1980**, *19*, 2619–2626.
(21) Søtofte, I. *Acta Chem. Scand.* **1976**, *A30*, 157–162.
(22) Königer-Ahlborn, E.; Müller, A.; Cormier, A. D.; Brown, J. D.; Nakamoto, K. *Inorg. Chem.* **1975**, *14*, 2009–2011.
(23) Bowmaker, G. A.; Boyd, P. D. W.; Campbell, G. K.; Zvagulis, M. *J. Chem. Soc., Dalton Trans.* **1986**, No. 6, 1065–1073.
(24) Clark, R. J. H.; Walton, J. R. *J. Chem. Soc., Dalton Trans.* **1987**, No. 6, 1535–1544.
(25) Makhyoun, M. A. *Polyhedron* **1988**, *7*, 2675–2678.
(26) Slater, J. C. *Phys. Rev.* **1951**, *18*, 385.
(27) Slater, J. C. *Quantum Theory of Molecules and Solids*; McGraw-Hill: New York, 1974; Vol. IV.
(28) (a) Johnson, K. H. *J. Chem. Phys.* **1966**, *45*, 3085. (b) Johnson, K. H. *Int. J. Quantum Chem.* **1967**, *1S*, 361. (c) Johnson, K. H. *Int. J. Quantum Chem.* **1971**, *4*, 153.
(29) Johnson, K. H. *Adv. Quantum Chem.* **1973**, *7*, 143.
(30) Watson, R. E. *Phys. Rev.* **1958**, *111*, 1108.

Table I. Interatomic Distances (au), Sphere Radii (au), and the α Exchange Values for the Different Thiomolybdate and Thiotungestate Complex Ions[a]

param	$[NiMo_2S_8]^{2-}$	$[PdMo_2S_8]^{2-}$	$[PtMo_2S_8]^{2-}$	$[NiW_2S_8]^{2-}$	$[PdW_2S_8]^{2-}$	$[PtW_2S_8]^{2-}$
α param for outer sphere	0.719	0.718	0.716	0.717	0.716	0.715
M′–S_b dist	4.212	4.346	4.535	4.220	4.416	4.479
Mo–S_b dist	4.209	4.209	4.209			
Mo–S_t dist	4.064	4.064	4.064			
W–S_b dist				4.218	4.171	4.205
W–S_t dist				4.065	4.186	4.186
sphere radius of (M′ = Ni, Pd, Pt)	2.318	2.341	2.574	2.310	2.345	2.526
sphere radius (Mo)	2.447	2.453	2.452			
sphere radius (W)				2.532	2.555	2.563
sphere radius (S_b)	2.464	2.467	2.478	2.443	2.444	2.441
sphere radius (S_t)	2.526	2.527	2.526	2.492	2.550	2.550
sphere radius of outer sphere	10.87	11.06	11.32	10.85	11.01	11.25
sphere radius of Watson sphere	10.91	11.16	11.43	10.96	11.12	11.36

[a] l_{max}(outer sphere) = 4, l_{max}(Pt, W) = 3, l_{max}(Ni, Pd, Mo) = 2, l_{max}(S) = 1; charge on Watson sphere = +2.

chosen as follows: l_{max} = 1 for the S atoms, l_{max} = 2 for the Ni, Pd, and Mo atoms, l_{max} = 3 for the W and Pt atoms, and l_{max} = 4 for the outer sphere. The choice of l_{max} = 1 around S and O is based on the study on thiomolybdates[15] and thiotungstates.[31] A similar study on oxohalochromates[32] uses l_{max} = 2 around the halogens and O, but the ordering of the orbitals and the bonding scheme are very much similar to the thiomolybdate and thiotungstate work. In the case of the central metal, l_{max} = 3 was chosen for the heavier elements W and Pt, in which quasirelativistic effects are expected to be more pronounced than in the Ni and Pd counterparts. Preliminary results on the relativistic stabilization of the LUMO in organometallic complexes such as pentamethylbismuth[33] indicate that the HOMO–LUMO gap is not very much affected by the inclusion of d and f partial waves around the Bi center. The atomic α values used in the calculations are those of Schwarz,[34] while a weighted average of these values was used in the outer-spherical and the interspherical regions. The amount of sphere overlap was determined by the Norman criteria,[35] in which the amount of sphere overlap is calculated in a manner that would satisfy the virial theorem. The multiple-scattering Xα method partitions a molecular cluster into atomic interspherical and outer-spherical regions. In the first and third regions, the potential is assumed to be spherically symmetrical and the wave functions are essentially polynomials multiplied by the corresponding spherical harmonics. The potential in the interspherical region is taken to be a constant, which leads to a set of Helmholtz equations, the solutions of which are the Bessel functions.[36] Proper matching of the wave function and its first derivative is enforced across the regions' boundaries, and an iterative procedure is started until the attainment of self-consistency. Unlike other computational methods, in which the ionization energies come out to be the negative of the orbital energy, the negative of the MS-Xα orbital energies do not result in a similar correspondence. For this reason, one normally uses the transition-state method of Slater[37] for an appropriate evaluation of the ionization and excitation energies.

Since some of the molecule ions under study contain either W or Pt or both, the use of a relativistic Hamiltonian is deemed necessary. This would entail the use of the Dirac equation or a variation of it.[38-45] The incorporation of the mass velocity and the Darwin term in the Hamiltonian has been shown by Martin[46] to provide a remarkable approximation to the Dirac–Hartree–Fock approach. Ziegler et al.[47] have proposed a perturbative approach to the relativistic Hamiltonian and have shown that the contraction of bonds is of a direct relativistic origin. Barthelat et al.[48] on the other hand, have presented a second-order representation of the Dirac equation and have shown that, for atomic calculations, the results compare favorably with the Dirac–Hartree–Fock approach. A variational approach to relativistic effects has been suggested by Almlöf et al.[49] in LCAO calculations, and results obtained on one-electron atoms are compared with Dirac–Hartree–Fock exact solutions.

It had been shown that for spherically symmetrically potentials in atomic regions in which the muffin-tin potential approximation is used, the relativistic Schrödinger equation would be a variant of the nonrelativistic description in which three additional terms will be included in the Hamiltonian. The radial wave function, $\Psi_k(\mathbf{r})$, in the Dirac equation may then be factored out into two-component spinors $g_k(r)$ and $f_k(r)$

$$\Psi_k(\mathbf{r}) = \begin{pmatrix} g_k(r) \\ f_k(r) \end{pmatrix} \tag{1}$$

in which k is a relativistic quantum number and in which $g_k(r)$ is the more important component of the radial part that includes the other component $f_k(r)$. The total wave function may then be obtained by multiplying the radial part with two-component spin angular functions (analogous to the spherical harmonics) that are indexed with the quantum number $K \equiv k, m$. The relativistic Schrödinger equation may be obtained by the solution of the matrix equation

$$\mathbf{H}_k|\Psi_k(\mathbf{r})\rangle = |0\rangle \tag{2}$$

where $\mathbf{H}_k$ is a 2 × 2 matrix operator that appears explicitly in the following analogous form of the above equation

$$\begin{bmatrix} \left(\frac{d}{dr} + \frac{1}{r} - \frac{k}{r}\right)c & (E - V(r)) \\ -\left(1 - \frac{(E - V(r))}{c^2}\right)c & \left(\frac{d}{dr} + \frac{1}{r} + \frac{k}{r}\right) \end{bmatrix} \begin{bmatrix} f_k(r) \\ g_k(r) \end{bmatrix} = \begin{pmatrix} 0 \\ 0 \end{pmatrix} \tag{3}$$

in which c is the speed of light in vacuum and k is the relativistic counterpart of the angular momentum quantum number. It is apparent that the above matrix equation reduces to the nonrelativistic analogue when the left-hand off-diagonal term in $\mathbf{H}_k$ approaches the speed of light. This is apparently true for light atoms and for the valence band regions of heavy atoms. The set of differential equations that result as a solution of the matrix equation are coupled and may be solved by eliminating $f_k(r)$. This would consequently lead to the relativistic Hamiltonian, $H_R(r)$. The relativistic Schrödinger equation would then be given by

$$H_R(r)\, rg_k(r) = [H_{NR}(r) + H_M(r) + H_D(r) + H_{SO}(r)]rg_k(r) = 0 \tag{4}$$

in which $H_{NR}(r)$ is the nonrelativistic prototype of the Schrödinger equation and is given by

(31) El-Issa, B. D.; Ali, A. A. M.; Zanati, H. Submitted for publication in *Int. J. Quantum Chem.*
(32) Miller, R. M.; Tinti, D. S.; Case, D. A. *Inorg. Chem.* **1989**, *28*, 2738–2743.
(33) El-Issa, B. D.; Pyykkö, P.; Zanati, H. In progress.
(34) Schwarz, K. *Phys. Rev. B* **1972**, *B5*, 2466.
(35) (a) Norman, J. G., Jr. *J. Chem. Phys.* **1974**, *61*, 4630. (b) Norman, J. G., Jr. *J. Mol. Phys.* **1976**, *31*, 1191.
(36) El-Issa, B. D. *Int. J. Quantum Chem.* **1981**, *S15*, 419.
(37) Slater, J. C. *Adv. Quantum Chem.* **1972**, *6*, 1.
(38) Boring, M.; Wood, J. H. *J. Chem. Phys.* **1979**, *71*, 32–41.
(39) Boring, M.; Wood, J. H. *J. Chem. Phys.* **1979**, *71*, 392–399.
(40) Koelling, D. D.; Harmon, B. N. *J. Phys. C: Solid State Phys.* **1977**, *10*, 3107–3114.
(41) Gollisch, H.; Fritsche, L. *Phys. Status Solidi B* **1978**, *86*, 145–150.
(42) Cowan, R. D.; Griffin, D. C. *J. Opt. Soc. Am.* **1976**, *66*, 1010–1014.
(43) Wood, J. H.; Boring, M.; Woodruff, S. B. *J. Chem. Phys.* **1981**, *74*, 5225–5233.
(44) Heera, V.; Seifert, G.; Ziesche, P. *J. Phys. B: At. Mol. Phys.* **1984**, *17*, 519–530.
(45) Pyykkö, P. *Chem. Rev.* **1988**, *88*, 563–594.
(46) Martin, R. L. *J. Phys. Chem.* **1983**, *87*, 750–754.
(47) Ziegler, T.; Snijders, J. G.; Baerends, E. J. *J. Chem. Phys.* **1981**, *74* (2), 1271–1284.
(48) Barthelat, J. C.; Pelissier, M.; Duran, Ph. *Phys. Rev. B* **1980**, *B21* (6), 1773–1785.
(49) Almlöf, J.; Feagri, K., Jr.; Grelland, H. H. *Chem. Phys. Lett.* **1985**, *114* (1), 53–57.

$$H_{NR} = \left[-\frac{d^2}{dr^2} + \frac{k(k+1)}{r^2} - (E - V(r)) \right] \quad (5)$$

$H_M(r)$ is the mass velocity term and is given by

$$H_M(r) = -\left(\frac{E - V(r)}{c} \right)^2 \quad (6)$$

$H_D(r)$ is the Darwin term and is given by

$$H_D(r) = -\left[\frac{B(r)}{c^2} \frac{dV}{dr} \left(\frac{d}{dr} - \frac{1}{r} \right) \right] \quad (7)$$

and $H_{SO}(r)$ is the spin–orbit correction term given by

$$H_{SO}(r) = -\left[\frac{B(r)}{c^2} \frac{dV}{dr} \left(\frac{k+1}{r} \right) \right] \quad (8)$$

where $B(r)$ is given by

$$B(r) = \left[1 + \frac{(E - V(r))}{c^2} \right]^{-1} \quad (9)$$

In this paper we refer to the $B(r)$ factors as mass–velocity parametric terms. In normal relativistic scattered-wave calculations, the spin–orbit term is left out of the Hamiltonian and hence the quasirelativistic acronym. Some authors, however, have included this correction as a perturbation term in post-SCF calculations.[43]

It is now established that the inclusion of relativistic corrections leads to a situation in which the s and p radial wave functions become contracted with a corresponding stabilization of the orbitals in contradistinction to d and f radial wave functions that become more diffuse with a corresponding destabilization of the orbitals. The amount of contraction (or expansion) is evidently proportional to ν/c; ν being the average velocity (in au) of an electron in a given orbital and c being the speed of light ($\equiv$137 au). Electrons that occupy the 1s orbital, for instance, have average speeds close to the number of protons in the nucleus and are thus most severely affected by these corrections. In molecular systems, the above arguments may be extended to molecular orbitals that have large contributions of s, p, d, and f components.

The implementation of the relativistic corrections in the Hamiltonian within the formalism of a muffin-tin potential and a statistical local exchange potential leads to the set of simultaneous equations that have the form[50]

$$A^{\gamma}_{\lambda\mu} T(\lambda,\alpha) - \sum_{\beta} \sum_{\lambda'\mu'} A^{\beta}_{\lambda'\mu'} G^{\gamma\beta}_{\lambda\mu,\lambda'\mu'}(\mathbf{R}_{\alpha\beta}) = 0 \quad (10)$$

in which $A^{\gamma}_{\lambda\mu}$ is the appropriate coefficient with respect to the γth atomic sphere, $G^{\tau\delta}_{\lambda\mu,\lambda'\mu'}(\mathbf{R}_{\tau\delta})$ is the geometric parameter that depends on the distance between the τth and the δth atomic spheres, λ and μ are indices that represent angular momentum and magnetic quantum numbers, respectively, and $T(\lambda,\alpha)$ is the scattering factor. The relativistic analogue of these factors may be given by

$$T(\lambda,\alpha) = \frac{[(B^{-1})_\alpha R(E;b_\alpha)\, \xi_\kappa'(\omega b_\alpha) - (\bar{B}^{-1})\, R'(E;b_\alpha)\, \xi_\kappa(\omega b_\alpha)]}{[(\bar{B}^{-1})\, R(E;b_\alpha)\, \mathcal{N}_\kappa'(\omega b_\alpha) - (B^{-1})_\alpha R'(E;b_\alpha)\, \mathcal{N}_\kappa(\omega b_\alpha)]} \quad (11)$$

in which b_α is the radius of the αth atomic sphere, $R(E;b_\alpha)$ is the spherically symmetrical radial function evaluated at $r = b_\alpha$ and is written explicitly as a function of the energy E, $R'(E;b_\alpha)$ is the appropriate first derivative of such a function, and $\mathcal{N}_\kappa(\omega b_\alpha)$, $\xi_\kappa(\omega b_\alpha)$, $\mathcal{N}_\kappa'(\omega b_\alpha)$, and $\xi_\kappa'(\omega b_\alpha)$ are spherical Bessel and Neumann functions and their first derivatives, respectively, evaluated at $r = b_\alpha$. The latter functions are solutions of the Helmholtz equation in the interspherical region in which the potential is proportional to the parameter ω. In the above equation, the mass velocity parametric terms are evaluated at $r = b_\alpha$ [the $(B^{-1})_\alpha$ term] and in the constant-potential region [the $(\bar{B}^{-1})$ terms]. It is apparent that in the limit as $B \to 1$, the above equation reduces to the nonrelativistic analogue

$$T(\lambda,\alpha) = [R(E;b_\alpha), \xi_\kappa(\omega b_\alpha)] / [R(E;b_\alpha), \mathcal{N}_\kappa(\omega b_\alpha)] \quad (12)$$

in which the square brackets denote the Wronskian of the two enclosed functions. The Wronskian, in essence, constitutes satisfying the boundary conditions that incident and scattered partial waves in the interspherical region are properly matched with numerical radial functions in the atomid (spherically symmetrical) regions. If the scattering factors and the structural parameters are represented by the matrices **T** and **G**, respectively, solutions to eq 10 may be obtained by solving a secular equation in which the roots of the determinant (**T**–**G**) are obtained by a judicious variation in the energy. Ionization and excitation energies are calculated by employing the transition-state method of Slater.[37]

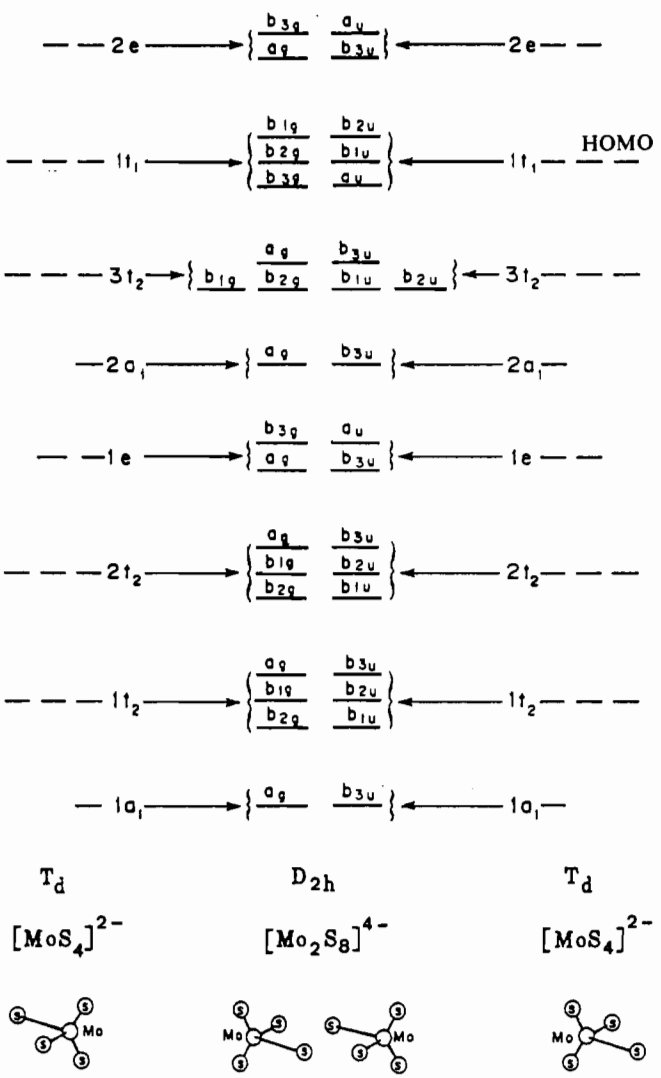

Figure 3. Interaction diagram that represents the transformed orbitals of the $[MoS_4]^{2-}$ moieties in a D_{2h} environment.

Results and Discussion

Much confusion in the proper representatiioin of the orbitals that ensues as a result of forming the complex ion has led to inaccuracies as to the type of excitation processes that prevails. There does not seem to be any motivation for referring to the orbitals in a tetrahedral environment when the actual environment has D_{2h} symmetry. Excitation from the $1t_1$ (HOMO) to the 2e (LUMO) orbital in $[MoS_4]^{2-}$ is definitely not the same as similar excitation from the HOMO to the LUMO in $[Ni(MoS_4)_2]^{2-}$. Perhaps the best approach for presenting a comprehensive theoretical study of these molecule ions is to attack the problem by referencing the $[M'(MoS_4)_2]^{2-}$ orbitals to the respective tetrahedral environment of the $[MoS_4]^{2-}$ moieties. This would constitute the transformation of the molecular orbitals of the $[MoS_4]^{2-}$ moieties from their tetrahedral environment when they are at large distances to the D_{2h} environment that prevails when the moieties are made to approach the central metal ion at the respective equilibrium distances. In general, the valence electron configuration of the central transition metal (Ni^{2+}, Pd^{2+}, Pt^{2+}) is represented by the $(n+1)s^0\, nd^8$ configuration. Under the D_{2h} symmetry, the d orbitals will be decomposed into the set ($b_{1g} + b_{2g} + b_{3g} + 2a_g$), while the s orbitals will be resolved into A_g symmetry. As a result of the transformation of the molecular orbitals of the $[MoS_4]^{2-}$ moieties from the tetrahedral to the D_{2h} environment in the preence

(50) El-Issa, B. D. Molecular Energy Levels Studied by the SCF–Xα Technique. Ph.D. Thesis, University of Manchester Institute of Science and Technology, 1980.

Scheme I

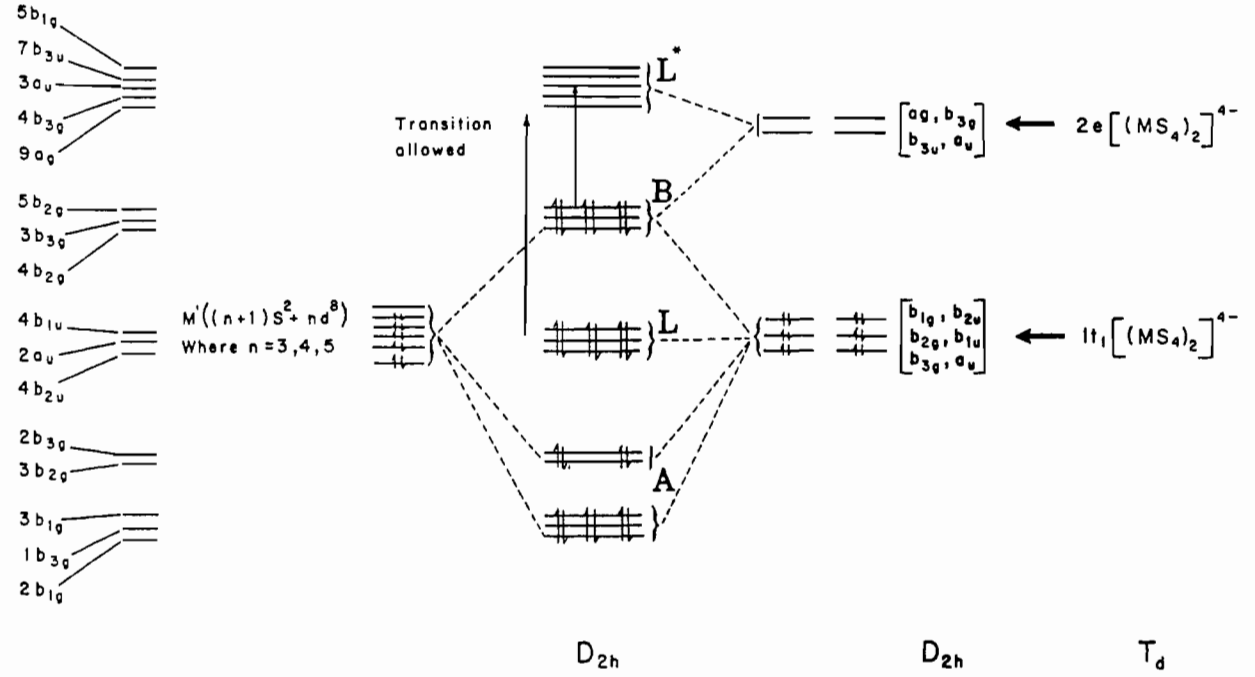

of the central metal ion, the a_1 and t_2 orbitals will be decomposed into the (a_g, b_{3u}) set and the (b_{1g}, b_{2g}, a_g, b_{1u}, b_{2u}, b_{3u}) set, respectively. On the other hand, the e and t_1 orbitals will be resolved under D_{2h} symmetry into two sets, namely (a_g, b_{3g}, a_u, b_{3u}) and (b_{1g}, b_{2g}, b_{3g}, b_{1u}, b_{2u}, a_u), respectively. An interaction diagram that represents the transformed orbitals of $[MoS_4]^{2-}$ in a D_{2h} environment is displayed in Figure 3. Figure 4 illustrates an interaction diagram that shows the bonding scheme between the central Ni 4s and 3d orbitals and the orbitals of the $[(MoS_4)_2]^{2-}$ moieties in a D_{2h} environment. In this figure we only display the correlation for orbitals in which the composiition is at least 10%. The orbitals that span the energy range from −1.49 to −1.38 Ry may be identified as localized 3s bases on the S moieties, with the set of orbitals that constitutes the bridging ligands occurring at lower energies. The originally occupied orbitals $2t_2$ and 1e of each $[MoS_4]^{2-}$ moiety contain appreciable Mo(d) character[15] and, in the D_{2h} environment, transform in such a way that would allow some of them to interact with the central Ni atom. The set of orbitals that have B_{1u}, B_{2u}, B_{3u}, and A_u symmetry remain nonbonding with variable admixtures of the Mo(d) bases. The 2e orbital (LUMO) of the $[MoS_4]^{2-}$ moieties transforms in the D_{2h} environment into a set of orbitals that have A_g, A_u, B_{3g}, and B_{3u} symmetry. In fact our results show that the LUMO in the complex ions $[M'(MS_4)_2]^{2-}$ in which M = Mo and M′ = Ni, Pd, Pt is $9a_g$ and is of preponderant $M(d_{x^2-y^2})$ character. A contour map that illustrates this orbital in $[Ni(MoS_4)_2]^{2-}$ is shown in Figure 5. As will be mentioned later, the introduction of a heavy metal for M′ leads to quasirelativistic effects that result in a reordering of the orbitals. In particular, the LUMO in $[Pd(WS_4)_2]^{2-}$ is $5b_{1g}$, which involves antibonding interaction between the $Pd(d_{xy})$ and the p orbitals of the bridging sulfurs, as may be verified in Figure 6. In the case of $[Pt(WS_4)_2]^{2-}$, however, the LUMO is $4b_{3g}$, which constitutes antibonding interaction between the $Pt(d_{yz})$ component and the S(p) orbitals. Figure 7 is an illustration of this orbital. Moreover, the $1t_1$ orbital of each $[MoS_4]^{2-}$ moiety, which constitutes only S(p) bases by symmetry, is transformed in a D_{2h} environment into a set of orbitals that have B_{1g}, B_{2g}, B_{3g}, B_{1u}, B_{2u}, and A_u symmetry. The highest six occupied orbitals in all the complex ions, in fact, have the same representations irrespective of the nature of the M and M′ center and are such that they constitute minimal contribution from the M center. The HOMO, however, is consistently $5b_{2g}$, which constitutes localized $M'(d_{xz})$ and ligand p character. This orbital in the case of $[Pt(MoS_4)_2]^{2-}$ is illustrated in Figure 8. The $3t_2$ orbitals may be analyzed in a similar manner. Finally, the $2a_1$ orbitals of the $[MoS_4]^{2-}$ moieties, which transform in the D_{2h} environment into a set of orbitals that have A_g and B_{3u} symmetry, constitute Mo(s), Mo(d), and S(p) character.

Table II. Main Constituents of the Different Molecular Orbitals As Represented in Scheme I

category	state	main constituents
L*	$5b_{1g}$	d(M′), S_b(p)
	$7b_{3u}$	d(M), S_b(p), S_t(p)
	$3a_u$	d(M), S_t(p), S_b(p)
	$4b_{3g}$	d(M), S_t(p)
	$9a_g$	d(M), S_t(p)
B	$5b_{2g}$	d(M′), S_t(p), S_b(p)
	$3b_{3g}$	d(M′), S_b(p), S_t(p)
	$4b_{2g}$	d(M′), S_t(p), S_b(p)
L	$4b_{1u}$	S_t(p)
	$2a_u$	S_b(p), S_t(p)
	$4b_{2u}$	S_t(p), S_b(p)
A	$2b_{3g}$	d(M′), d(M), S_t(p)
	$3b_{2g}$	d(M′), S_b(p), S_t(p)
	$3b_{1g}$	d(M′), d(M), S_b(p)
	$1b_{3g}$	d(M′), d(M), S_b(p)
	$2b_{1g}$	d(M′), d(M), S_b(p)

In a manner similar to that reported by Müller,[5] a quantitative MO scheme (Scheme I) for the class of ions $[M'(MS_4)]^{2-}$ (M′ = Ni, Pd, Pt; M = Mo, W) may be suggested. In this scheme we assume that the most important interaction occurs between the central metal $(n + 1)s^2$ and nd^8 electrons and the orbitals of the ligand moieties of the triply degenerate occupied $1t_1$ orbitals and the doubly degenerate 2e virtual orbitals (Table II). It is obvious from Table II, that the respective MO's of the ligands and the central metal may be categorized into sets of orbitals that may be associated with M′ and M metal d character and others that contain predominantly S(p) character. In Scheme I, the different categories are identified as A, L, B, and L*, in which A represents a set of orbitals that is mainly consistent of mixed metal–ligand character, L represents a set that constitutes MO's that have predominant S(p) character, B represents a set that constitutes central metal d character, and L* represents a set of unoccupied orbitals that is predominantly composed of M(d) bases. Within the L* category, the $5b_{1g}$ orbital may be singled out to be the only orbital that contains predominant central metal character. Scheme I also depicts the highest occupied MO to be predominantly of central metal d character, while the lowest occupied orbitals to be of predominant ligand character with large contribution from the Mo(4d) or the W(5d) components. In the

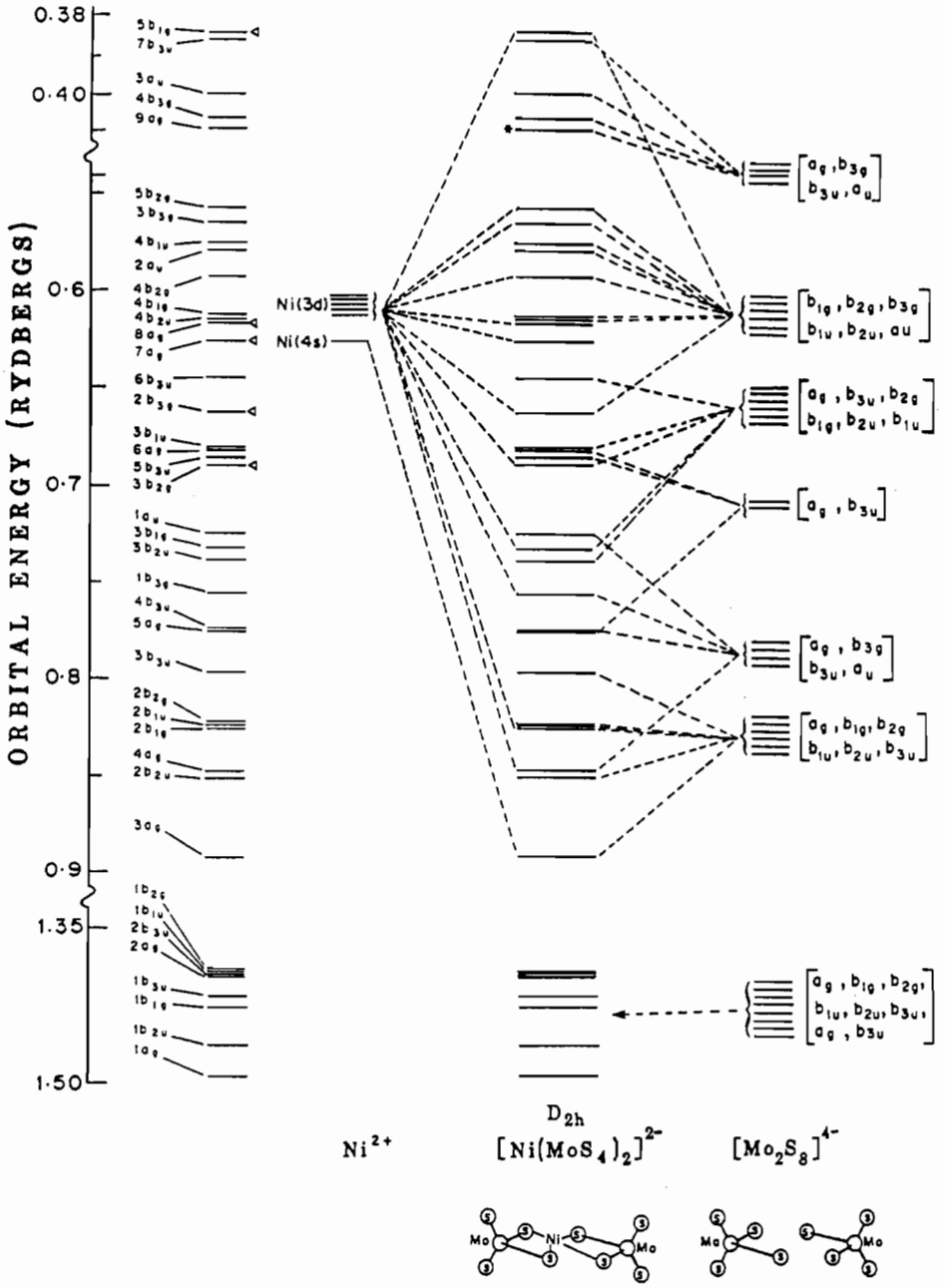

Figure 4. Interaction diagram that shows the MS–Xα orbital energies (in rydbergs) for the $[Ni(MoS_4)_2]^{2-}$ complex ion. The LUMO is indicated by an asterisk.

case of the $[Ni(WS_4)_2]^{2-}$ and $[Pd(WS_4)_2]^{2-}$ complex ions, $5b_{1g}$ is variant from the other complexes in which the LUMO has either A_g or B_{3g} symmetry that constitutes predominantly d character of either tungsten or molybdenum with admixtures of sulfur (p) bases. Since the dipole vector in a D_{2h} environment may be resolved into the B_{1u}, B_{2u}, and B_{3u} IRs, the only allowed transition from category B are those that involve excitations from the b_{2g} to the a_u or b_{3u} orbitals. Transitions are also allowed from the b_{3g} to the a_u orbitals. However, the first allowed transitioin to the LUMO occurs from the nonbonding ligand orbitals that have B_{1u} and B_{2u} symmetry and is basically a charge transfer process. This agrees well with results reported by Clark and Walton,[24] in which they suggest that at least one of the excitation bands corresponds to a ($S_b \rightarrow M$ = Mo, W) charge-transfer band.

The MS–Xα orbital energies in rydbergs and the corresponding charge composition for the thiomolybdate and thiotungstate complexes of Ni, Pd, and Pt are displayed in Table III and Tables IV–VIII (supplementary material). The LUMO of the thiomolybdate complexes of Ni, Pd, and Pt is $9a_g$ and is antibonding with a preponderant Mo($d_{x^2-y^2}$) and S_b(p) character. This result is in good agreement with previous theoretical calculations that had been reported for the $[Ni(MoS_4)_2]^{2-}$ complex ion.[23] In contrast, the LUMO of $[Ni(WS_4)_2]^{2-}$ and $[Pd(WS_4)_2]^{2-}$ is the $5b_{1g}$ orbital, while for $[Pt(WS_4)_2]^{2-}$ it is the $4b_{3g}$ orbital. The $5b_{1g}$ MO of the thiotungstate complexes of Ni and Pd represents antibonding interaction that is mainly associated with M'-(d_{xy})–S(p) components, while the antibonding $4b_{3g}$ orbital of $[Pt(WS_4)_2]^{2-}$ is basically composed of W(d_{xz}) and S_t(p) character. It is possible to explain the discrepancy in the ordering of the LUMO in the thiotungstate complexes on the basis of quasirelativistic effects. It is well-known that quasirelativistic factors (greater in the case of Pt than in Ni or Pd) will result in having the d orbitals become more diffuse with a corresponding upward shift in the orbital energy.[51] Consequently, the MO's that have predominant d character will be raised in energy as in the $5b_{1g}$ orbital, while those that have predominant ligand character will only slightly change.[52] In order to qualify our result, we have repeated the calculation for the $[Pt(WS_4)_2]^{2-}$ complex without

(51) Koga, N.; Morokuma, K. *J. Am. Chem. Soc.* **1986**, *108*, 6136–6144.
(52) Geiger, W. E., Jr.; Allen, C. S.; Mines, T. E.; Senftleber, F. C. *Inorg. Chem.* **1977**, *16*, 2003–2008.

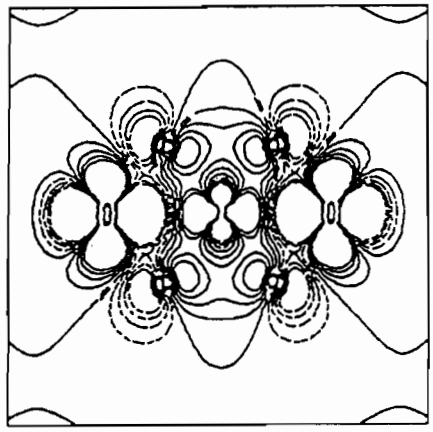

Figure 5. Contour map of the $9a_g$ (LUMO) orbital in $[Ni(MoS_4)_2]^{2-}$, which shows antibonding interaction between the $Ni(d_{x^2-y^2})$, $Mo(d_{x^2-y^2})$ and $S_b(p)$ components in the xy plane.

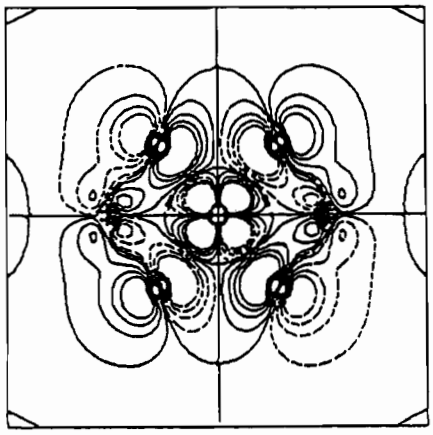

Figure 6. Contour map of the $5b_{1g}$ (LUMO) orbital in $[Pd(WS_4)_2]^{2-}$, which involves antibonding interaction between the $Pd(d_{xy})$ and $S_b(p)$ components in the xy plane.

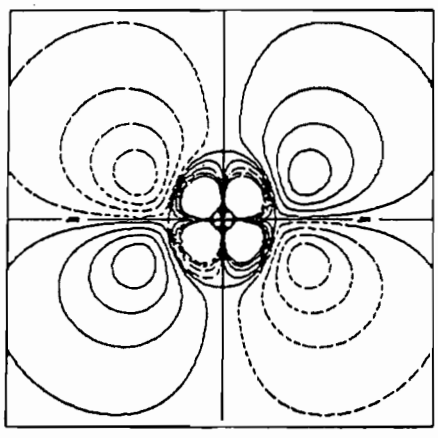

Figure 7. Contour map of the $4b_{3g}$ (LUMO) orbital in $[Pt(WS_4)_2]^{2-}$, which shows antibonding interaction between the $Pt(d_{yz})$ and the S(p) components in the yz plane.

incorporating the mass velocity and the Darwin corrections in the total Hamiltonian (procedure B). Another calculation was performed in which the quasirelativistic corrections were not incorporated around the Pt sphere (procedure C). The results are summarized in Figure 9, in which a comparison is made between the relativistic (procedure A) and the nonrelativistic (procedures B and C) calculations. It is apparent from the figure that the set of virtual orbitals that constitute mainly M and M′ character are shifted down in energy (i.e. have been stabilized) when the relativistic corrections are discarded. The reordering of the occupied orbitals follows similar trends in which orbitals that have large contributions from the d component of Pt and W are stabilized whereas orbitals that constitute appreciable contribution from the s component of Pt and W are destabilized. It is interesting to note that in procedure C, in which quasirelativisitic corrections are incorporated on all the spheres less Pt, the position of the $5b_{1g}$ orbital is seen to be shifted down in energy to a level that makes it the LUMO, as in the case of the Ni and Pd complex ions. One may attribute the difference in the description of the LUMO in the case of $[Ni(MoS_4)_2]^{2-}$ and $[Ni(WS_4)_2]^{2-}$ ($9a_g$ and $5b_{1g}$, respectively) to the quasirelativistic corrections in which the orbitals that are predominantly W(d) in character are shifted to higher energies compared to similar orbitals in the case of the molybdate analogue in which the relativistic effects are less marked. Since the incorporation of quasirelativistic factors leads to a contraction in the s orbitals, one expects a similar contraction in the radial distribution function for the s component of a heavy metal in a given molecular orbital. Indirect relativistic effects, however have been reported by Schwarz et al.[53] to influence the

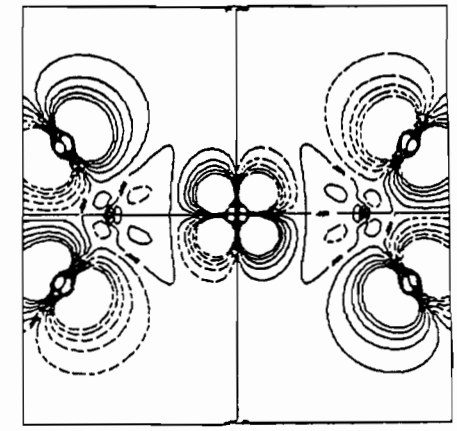

Figure 8. Contour map of the $5b_{2g}$ orbital (HOMO) in $[Pt(MoS_4)_2]^{2-}$, which constitutes a localized $Pt(d_{xz})$ and $S_t(p)$ components in the xz plane.

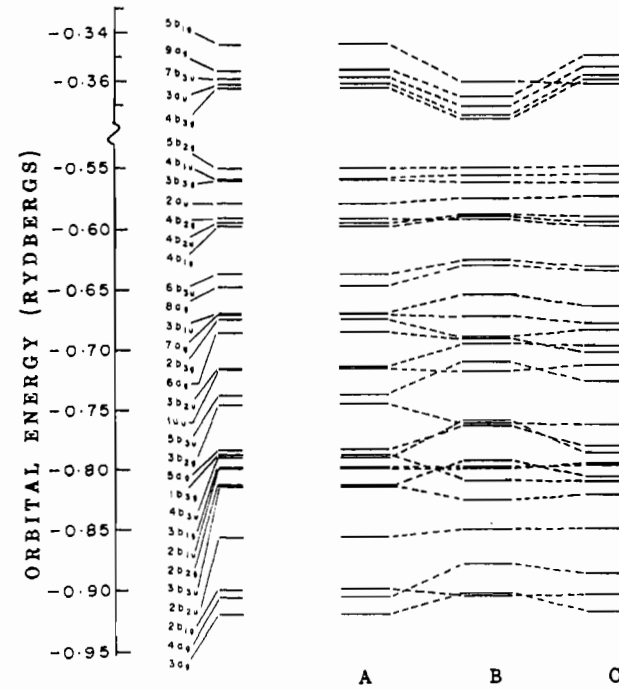

Figure 9. Correlation diagram that shows the MS–Xα orbital energies (in rydbergs) for $[Pt(WS_4)_2]^{2-}$, where in procedure A the quasirelativistic corrections were incorporated in the total Hamiltonian, in procedure B the quasirelativistic corrections were not incorported in the total Hamiltonian, andnd in procedure C the quasirelativistic corrections were not incorporated around the Pt sphere.

(53) Schwarz, W. H. E.; Van Wezenbeek, E. M.; Baernds, E. J.; Snijders, J. G. *J. Phys. B: At., Mol. Opt. Phys.* **1989**, *22*, 1515.

Table III. Molecular Orbital Energies (Ry) and Charge Composition of the Respective Molecular Orbitals of $[Ni(MoS_4)_2]^{2-}$ in a D_{2h} Environment[a]

MO's	orbital energies	Ni		Mo		S_b		S_t	
		s	d	s	d	s	p	s	p
$5b_{1g}$	−0.3838		0.409		0.007	0.005	0.130		0.007
$7b_{3u}$	−0.3854				0.306		0.050		0.044
$3a_u$	−0.3996				0.317		0.032		0.059
$4b_{3g}$	−0.4050		0.010		0.317		0.021		0.068
$9a_g$	−0.4082*	0.022	0.065		0.328		0.016		0.045
$5b_{2g}$	−0.5574		0.203				0.095		0.104
$3b_{3g}$	−0.5645		0.378				0.095		0.060
$4b_{1u}$	−0.5776						0.015		0.233
$2a_u$	−0.5798				0.002		0.146		0.103
$4b_{2g}$	−0.5929		0.280		0.001		0.031		0.142
$4b_{1g}$	−0.6131						0.036		0.200
$4b_{2u}$	−0.6167			0.006			0.030		0.204
$8a_g$	−0.6174	0.003	0.759	0.015	0.022		0.016		0.023
$7a_g$	−0.6260	0.088	0.867				0.008		0.002
$6b_{3u}$	−0.6454			0.019	0.018		0.087		0.121
$2b_{3g}$	−0.6625		0.462		0.078		0.011		0.084
$3b_{1u}$	−0.6810				0.001		0.189		0.041
$6a_g$	−0.6819	0.008	0.043		0.108		0.019		0.155
$5b_{3u}$	−0.6859			0.044	0.105	0.005	0.107		0.060
$3b_{2g}$	−0.6905		0.502		0.003		0.087		0.028
$1a_u$	−0.7278				0.195		0.070		0.082
$3b_{1g}$	−0.7356		0.312		0.125	0.001	0.095		0.011
$3b_{2u}$	−0.7408				0.013	0.003	0.199		0.009
$1b_{3g}$	−0.7585		0.161		0.120		0.112		0.072
$4b_{3u}$	−0.7767			0.034	0.095	0.002	0.116	0.002	0.049
$5a_g$	−0.7771		0.046	0.056	0.072		0.015	0.007	0.151
$3b_{3u}$	−0.7989			0.006	0.183	0.002	0.028	0.006	0.116
$2b_{2g}$	−0.8240		0.018		0.191		0.012	0.008	0.127
$2b_{1u}$	−0.8248				0.192		0.014	0.008	0.128
$2b_{1g}$	−0.8268		0.250		0.082	0.010	0.131		0.005
$4a_g$	−0.8485	0.033	0.100	0.017	0.096	0.004	0.139		0.012
$2b_{2u}$	−0.8523				0.168		0.154		0.004
$3a_g$	−0.8939	0.119	0.086	0.002	0.073	0.006	0.149		0.006
$1b_{2g}$	−1.3844				0.040			0.219	0.003
$1b_{1u}$	−1.3847				0.040			0.219	0.003
$2b_{3u}$	−1.3889			0.010	0.028	0.018		0.204	0.003
$2a_g$	−1.3897			0.018	0.022	0.001		0.221	0.003
$1b_{3u}$	−1.4153			0.025	0.004	0.206	0.003	0.018	
$1b_{1g}$	−1.4213		0.041		0.028	0.217	0.003		
$1b_{2u}$	−1.4621				0.022	0.224	0.002		
$1a_g$	−1.4900	0.058	0.016	0.013	0.006	0.214	0.004	0.001	
net pop		0.618	9.048	0.530	4.266	1.826	4.436	1.826	4.688

[a] The LUMO is indicated by an asterisk.

s and p shells. These effects have been reported to be quite large and of either sign. In our case, the relativistic effects are seen to be responsible for reordering of the virtual orbitals in the case of the nickel thiotungstate complex ion. Relativistic and nonrelativistic calculations on the isolated $[WS_4]^{2-}$ moiety show that the relativistic HOMO–LUMO excitation energy is 3.5 eV, as compared with the nonrelativistic value of 3.30 eV. This is to be compared with similar calculations performed on the isolated $[MoS_4]^{2-}$ ion in which the relativistic and nonrelativistic excitation energies come out to 2.76 and 2.69 eV, respectively. Since in both models the HOMO is pure ligand p in character, the difference of 0.78 eV between the excitation energy of the thiomolybdate and thiotungstate complex ions must therefore be traced to the seemingly greater relativistic destabilization of the LUMO in the case of the thiotungstate complex ion.

The HOMO for the six complex ions is $5b_{2g}$, which is of localized $M'(d_{xz})$, $S_t(p)$, and $S_b(p)$ nature. Taking into consideration the charge composition of the M′(d), $S_t(p)$, and $S_b(p)$ bases that correspond to the $5b_{2g}$ orbital, one may conclude the following: (a) within the thiomolybdate and the thiotungstate complex ions, the trends of the charge composition of the M′(d) will be in the order Ni > Pt > Pd, (b) the charge composition of the M′(d) component for the thiomolybdate complex ions will be greater than the thiotungstate complex ions, and (c) the charge composition of the $S_t(p)$ orbitals of the thiotungstates is greater than the analogous orbitals of the thiomolybdate complexes, which is contrary to the $S_b(p)$ orbitals. According to the charge compositioin of the orbitals in the $[Ni(MoS_4)_2]^{2-}$ complex ion (Table III), one may assign the $7a_g$ orbital to the MO that consists of localized $Ni(d_{z^2})$ with a small admixture from the $S_t(p)$ basis, whereas the $8a_g$ orbital may be assigned to one that constitutes localized $Ni(d_{x^2-y^2})$ and a small contribution from the $Mo(d_{x^2-y^2})$ and $S_p(p)$ orbitals. Our results concerning the $7a_g$ orbital are different from those reported by Makhyoun for the $[W_3S_8]^{2-}$ complex,[25] in which the $7a_g$ orbital was identified as a W_c-(d_{z^2})–$W_t(d_{z^2})$ σ bond. We may point out here, however, that the assignment of the axes used in that paper is not consistent with the conventional description used for the d components. In Figure 10, we display a contour map that describes the $7a_g$ orbital in the xz plane for the $[Ni(MoS_4)_2]^{2-}$ complex ion, where the contribution from the Mo(d) component is seen to be minimal. The stability of the complex ions under study and the apparent reported short distance between the metal centers may be attributed to σ and π interactions that involve the $d_{x^2-y^2}$ orbitals in the former and the d_{yz}, d_{xz}, and d_{xy} orbitals in the latter. A typical orbital that represents a π bond is $3b_{1g}$ in $[Ni(MoS_4)_2]^{2-}$ and is depicted in Figure 11, which is drawn in the xy plane. Another important interaction that may be considered is that which involves the d_{yz} orbital of the metal centers. The bonding representation of such an orbital would constitute a δ bond that involves the d_{yz} orbitals on the three metal centers. The $1b_{3g}$ is a prototype of such a representation and would presumably have a high electron density in a plane that crosses the yz plane at 45°. In an attempt to construe the evolution of the electron density of this orbital during

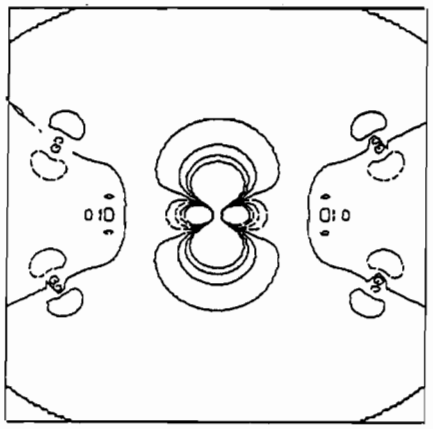

Figure 10. Contour map that describes the $7a_g$ orbital of $[Ni(MoS_4)_2]^{2-}$ in the xz plane, which consists of localized $Ni(d_{z^2})$ and $S_t(p)$ orbitals.

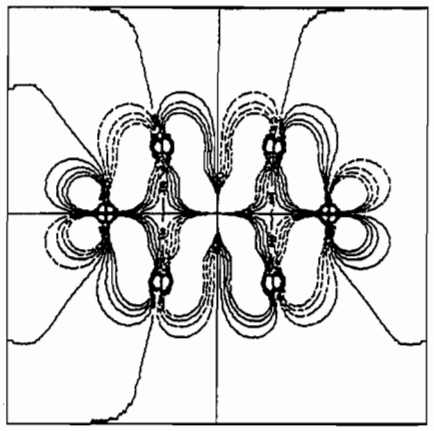

Figure 11. Contour map of the $3b_{1g}$ orbital of $[Ni(MoS_4)_2]^{2-}$, which represents a π-bonding interaction between the $Ni(d_{xy})$ and the $Mo(d_{xy})$ components in the xy plane.

the SCF procedure, we define the differential in the electron density (Γ_d) as

$$\Gamma_d = \Psi^2_{1b_{3g}}(\text{converged}) - \Psi^2_{1b_{3g}}(\text{initial}) \qquad (13)$$

in which $\Psi_{1b_{3g}}$(initial) repesents the molecular wave function of the $1b_{3g}$ orbital after one iteration and the $\Psi_{1b_{3g}}$(converged) represents such a wave function after the attainment of self-consistency.[54] Figure 12 is a representation of $\Psi^2_{1b_{3g}}$(initial) (Figure 12a), $\Psi^2_{1b_{3g}}$(converged) (Figure 12b), and Γ_d (Figure 12c). It is evident from the figure that during the SCF procedure, the electron density around the Ni center is redistributed in a manner that would allow the development of a δ bond. The interaction between the $M'(d_{xz})$ bases and the $[MS_4]^{2-}$ moieties will generally produce five occupied orbitals; the highest being the antibonding (HOMO) orbital. Inspection of the reported charge compositiion (Table III) reveals the fact that the $3b_{2g}$ and $4b_{2g}$ orbitals are of a localized $M'(d_{xz})$ and S(p) nature and that the $2b_{2g}$ orbital is a bonding MO that results from the interaction of the $M'(d_{xz})$ with the $M(d_{xz})$ and $S_t(p)$ components. It is important to note that under the D_{2h} environment, the occupied 1e orbital of the $[MS_4]^{2-}$ moiety transforms in a manner that would result in antibonding interaction between the two $[MS_4]^{2-}$ moieties. The contour map shown in Figure 13a is a representation of this orbital, drawn in the xy plane, and is to be compared with the contour map of the 1e orbital shown in Figure 13b, which is taken in a plane that contains the S moieties.

The analysis of the charge composition of the lowest eight molecular orbitals which consist of localized sulfur (s) character establishes the fact that orbitals of preponderant S_b character (namely, $1a_g$, $1b_{2u}$, $1b_{1g}$, and $1b_{3u}$) are consistently more stable than the corresponding orbitals that constitute S_t character (namely, $2a_g$, $2b_{3u}$, $1b_{1u}$, and $1b_{2g}$). The calculated net charges of the S_b and the S_t moieties (Table IX) predict the S_b moieties to carry less negative charge than the corresponding S_t counterparts. This may be attributed to the strong donation of charge from S_b to the central metal through the bridging bonds. In Table X, we display the net charge acquired by the central metal and the amount of charge donated from the $[MS_4]^{2-}$ moieties to the M′ center. The negative charge acquired by the M′ center is only artifactual since the normal procedure in multiple-scattering calculation is to partition the interspherical charge equally among the different centers, which normally leads to net negative charges carried by metal centers. It is obvious, however, that although the net charge carried by the metal centers comes out to be aberrant in value, systematic trends within a given class of complex ions regarding such a charge will be expected to be a factual representation. The net charge carried by the central metal in the $[Ni(MoS_4)_2]^{2-}$, $[Pd(MoS_4)_2]^{2-}$, and $[Pt(MoS_4)_2]^{2-}$ complexes is calculated to be −0.364 e, +0.012 e, and −0.318 e, respectively, whereas similar results regarding the thiotungstate complexes may be consulted from Table X. One may explain this discrepancy by the effective nuclear charge carried by the central metal as a result of the inclusion of the 4f electrons in the case of the Pt analogues. The effective nuclear charge on the metal centers, therefore, is expected to follow the trend Ni > Pt > Pd, and this nonfurtiously explains why the amount of charge donation to the Pt center is greater than that to Pd. This evidently leads to a case in which the Pt center will carry a net charge less than that of the Pd center. Although, one expects the orbital energies of the Pt complexes to be lower in value than those of the corresponding Pd complexes as a result of the increase in the effective nuclear charge, a contradistinctive trend will be expected as a result of the inclusion of quasirelativistic factors which dominate in the

Table IX. Net Charge on the Bridging and Terminal Sulfur Centers for the Different Thiomolybdate and Thiotungstate Complex Ions

complex	S_b	S_t
$[Ni(MoS_4)_2]^{2-}$	−0.275	−0.469
$[Pd(MoS_4)_2]^{2-}$	−0.359	−0.444
$[Pt(MoS_4)_2]^{2-}$	−0.297	−0.440
$[Ni(WS_4)_2]^{2-}$	−0.237	−0.437
$[Pd(WS_4)_2]^{2-}$	−0.250	−0.494
$[Pt(WS_4)_2]^{2-}$	−0.202	−0.482

Table X. Net Charge (in Electronic Charge Units) Acquired by the Central Metals of the Thiomolybdate and Thiotungstate Complex Ions (a) and Net Charge (in Electronic Charge Units) Donated by the Ligand Moieties to the Central Metal (b)

	$[M'(MoS_4)_2]^{2-}$		$[M'(WS_4)_2]^{2-}$	
M′	a	b	a	b
Ni	−0.364	2.364	−0.318	2.318
Pd	+0.012	1.989	+0.056	1.944
Pt	−0.318	2.318	−0.253	2.253

Table XI. Calculated and Experimental Excitation Energies (μm^{-1}) of Allowed Transitions to the LUMO in the Different Thiomolybdate and Thiotungstate Complex Ions

complex ion	excitation	MS−Xα	exptl[a]
$[Ni(MoS_4)_2]^{2-}$	$4b_{1u} \rightarrow 9a_g$	2.003	1.96
	$4b_{2u} \rightarrow 9a_g$	2.405	
$[Pd(MoS_4)_2]^{2-}$	$4b_{1u} \rightarrow 9a_g$	1.971	2.09
	$4b_{2u} \rightarrow 9a_g$	2.339	2.13
$[Pt(MoS_4)_2]^{2-}$	$4b_{1u} \rightarrow 9a_g$	1.890	2.16
	$4b_{2u} \rightarrow 9a_g$	2.265	
$[Ni(WS_4)_2]^{2-}$	$4b_{2u} \rightarrow 5b_{1g}$	2.854	2.36
	$6b_{3u} \rightarrow 5b_{1g}$	3.124	2.65
$[Pd(WS_4)_2]^{2-}$	$4b_{2u} \rightarrow 5b_{1g}$	2.367	2.51
	$6b_{3u} \rightarrow 5b_{1g}$	2.677	2.76
$[Pt(WS_4)_2]^{2-}$	$4b_{1u} \rightarrow 4b_{3g}$	2.291	2.32
	$4b_{2u} \rightarrow 4b_{3g}$	2.656	2.42, 3.16

[a] Clark, R. J. H.; Walton, J. R. *J. Chem. Soc., Dalton Trans.* **1987**, No. 6, 1535–1544.

(54) El-Issa, B. D. *J. Chem. Soc., Chem. Commun.* **1989**, 290–293.

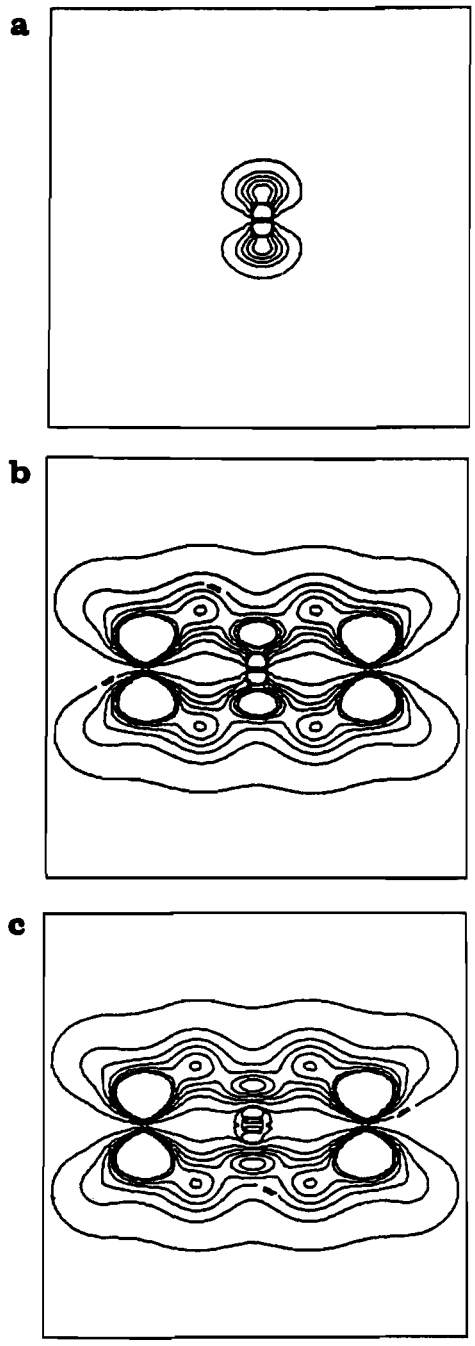

Figure 12. (a) Contour map that represents the Ψ^2_{1b3g}(initial) for the $[Ni(MoS_4)_2]^{2-}$ complex ion in a plane that crosses the *yz* plane at 45°. (b) Contour map that represents the Ψ^2_{1b3g}(converged) for the $[Ni(MoS_4)_2]^{2-}$ complex ion in a plane that crosses the *yz* plane at 45°. (c) Contour map that represents the differential in the electron Γ_d for the $[Ni(MoS_4)_2]^{2-}$ complex ion in a plane that crosses the *yz* plane at 45°.

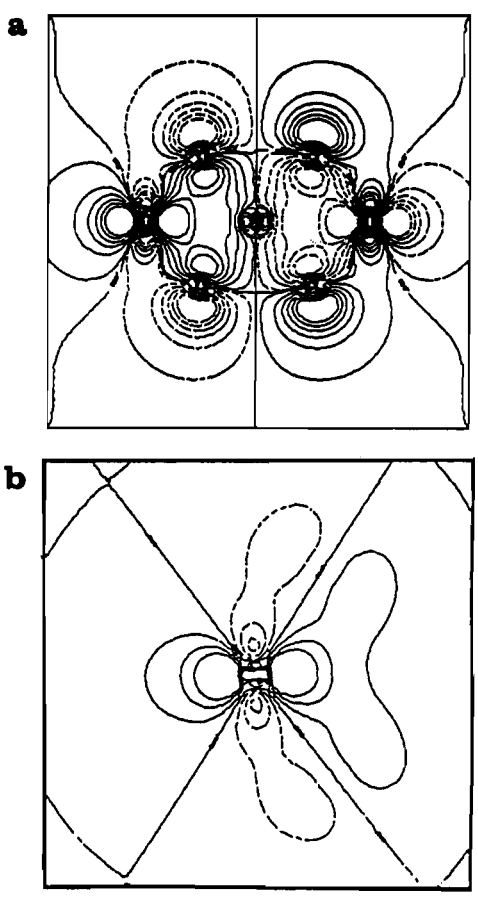

Figure 13. (a) Contour map of the $4b_{3u}$ orbital in $[Ni(MoS_4)_2]^{2-}$, which represents the antibonding interaction between the Mo($d_{x^2-y^2}$) and S_b(p) components of the two $[MS_4]^{2-}$ moieties, drawn in the *xy* plane. (b) Contour map of the occupied 1e orbital of the $[MS_4]^{2-}$ moiety, which shows a π-bonding interaction between the Mo($d_{x^2-y^2}$) and the ligand p orbitals. This map is drawn in a plane that contains the S ligands.

case of the Pt complexes. In Figure 14 we compare the orbital energies that constitute d character on the central metal in the case of the thiomolybdate complexes and the upper shift in the energy of these orbitals in the case of the Pt complexes is attributed to relativistic corrections.

In Table XI we report the longest wavelength transition bands to the LUMO in the $[M'(MS_4)_2]^{2-}$ complex ions. For the thiomolybdate complexes, the promotion of electrons to the LUMO ($9a_g$) is Laporte allowed from orbitals that have B_{1u}, B_{2u}, and B_{3u} symmetry. In the case of the thiotungstate complexes of Ni and Pd, the transition of electrons to the LUMO ($5b_{1g}$) is only allowed from orbitals that have B_{2u} or B_{3u} symmetry, while for the $[Pt(WS_4)_2]^{2-}$ complex ion the excitation of electrons to the LUMO ($4b_{3g}$) is allowed from the orbitals that have B_{1u} and B_{2u} symmetry. In this table we also report the longest wavelength excitation energy for the complex ions under study by using the transition-state method of Slater.[37] The experimental value of this band in the series $[Ni(MoS_4)_2]^{2-}$, $[Pd(MoS_4)_2]^{2-}$, and $[Pt(MoS_4)_2]^{2-}$ occurs at 1.96, 2.09, and 2.16 μm^{-1}, respectively, and is assigned to the $t_1 \rightarrow e$ transition of the free "$[MS_4]^{2-}$" ligand, which translates in our case to an allowed transition from $4b_{1u}$ to $9a_g$ (LUMO) and is calculated to be 2.003, 1.971, and 1.890 μm^{-1}, respectively. Although the experimental promotion energies are reported to increase along that series, our results predict a reversed trend. Considering a ± 0.2 μm^{-1} as an acceptable experimental error, the calculated excitation energies compare very favorably with the experimental counterparts. The experimental longest wavelength excitation energy for the thiotungstate complexes is reported at 2.36, 2.51, and 2.32 μm^{-1} for the series $[Ni(WS_4)_2]^{2-}$, $[Pd(WS_4)_2]^{2-}$, and $[Pt(WS_4)_2]^{2-}$ and compare favorably with the calculated values at 2.854, 2.367, and 2.291 μm^{-1}, respectively. This excitation, however, does not involve the promotion to the $9a_g$ orbital as in the case of the thiomolybdate complexes, and except for the Pt case, such an excitation may be described as an intra-charge-transfer process that involves the d orbitals of the central metal. The case of Pt remains outstanding because of the incorporation of the quasirelativistic corrections, as had been mentioned earlier. It is important, however, to note that the reported experimental splitting of the longest wavelength transition band (≈ 0.30 μm^{-1}) in the case of nickel and palladium thiotungstates may be attributed to the fact that more than one allowed excitation band may occur from the t_1 orbital of the $[MS_4]^{2-}$ to the e orbitals in a proper D_{2h} environment. Such an excitation could, for instance, occur from $6b_{3u}$ to $5b_{1g}$ and is calculated to be 3.124 and 2.677 μm^{-1}, respectively, for the complex ions $[Ni(WS_4)_2]^{2-}$ and $[Pd(WS_4)_2]^{2-}$. The difference between this promotion energy and the $4b_{2u} \rightarrow 5b_{1g}$ counterparts is ≈ 0.30 μm^{-1} and is very close to the observed experimental splitting. There

Table XII. MS-Xα Ionization Energies (eV) for the Highest Occupied Molecular Orbitals of the Different Thiomolybdate and Thiotungstate Complex Ions

complex	I_1	I_2	I_3	I_4	I_5
$[Ni(MoS_4)_2]^{2-}$	$5b_{2g}$ (9.26)	$3b_{3g}$ (9.47)	$4b_{1u}$ (9.52)	$2a_u$ (9.55)	$4b_{2g}$ (9.80)
$[Pd(MoS_4)_2]^{2-}$	$5b_{2g}$ (9.54)	$4b_{1u}$ (9.69)	$3b_{3g}$ (9.76)	$2a_u$ (9.88)	$4b_{2u}$ (10.1)
$[Pt(MoS_4)_2]^{2-}$	$5b_{2g}$ (9.30)	$3b_{3g}$ (9.38)	$4b_{1u}$ (9.54)	$2a_u$ (9.70)	$4b_{2g}$ (9.83)
$[Ni(WS_4)_2]^{2-}$	$5b_{2g}$ (8.90)	$3b_{3g}$ (9.14)	$4b_{1u}$ (9.13)	$2a_u$ (9.22)	$4b_{2g}$ (9.44)
$[Pd(WS_4)_2]^{2-}$	$5b_{2g}$ (9.22)	$4b_{1u}$ (9.30)	$3b_{3g}$ (9.50)	$2a_u$ (9.53)	$4b_{2u}$ (9.74)
$[Pt(WS_4)_2]^{2-}$	$5b_{2g}$ (9.11)	$4b_{1u}$ (9.24)	$3b_{3g}$ (9.26)	$2a_u$ (9.49)	$4b_{2g}$ (9.77)

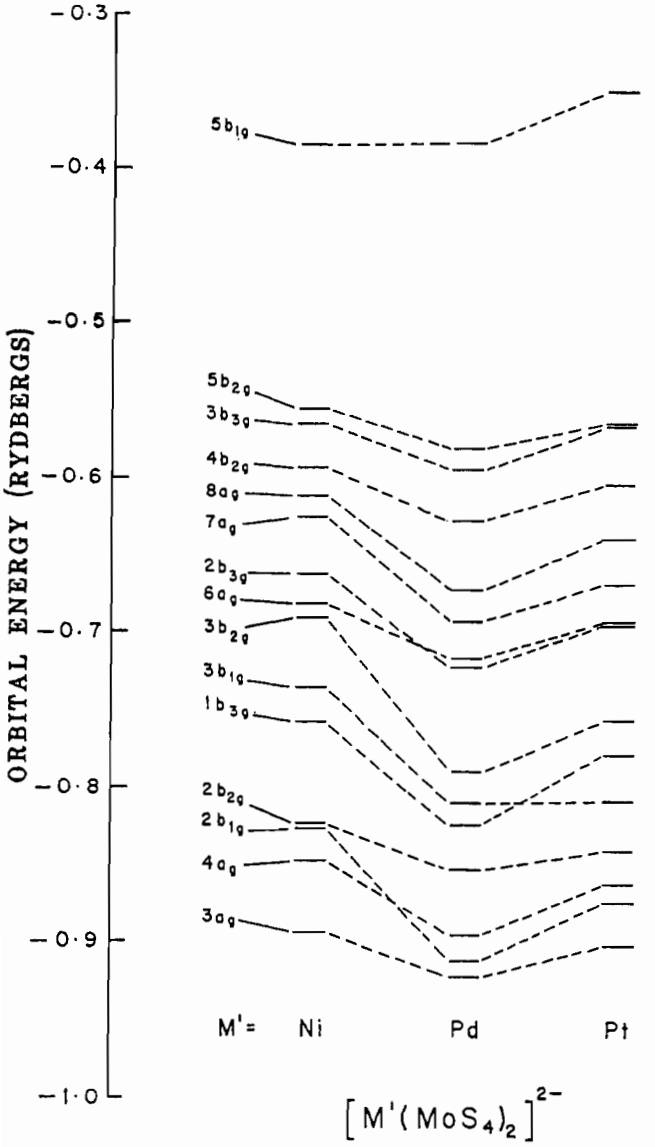

Figure 14. Comparison between the orbitals energies that contain d character of the central metal in the case of the thiomolybdate complex ions.

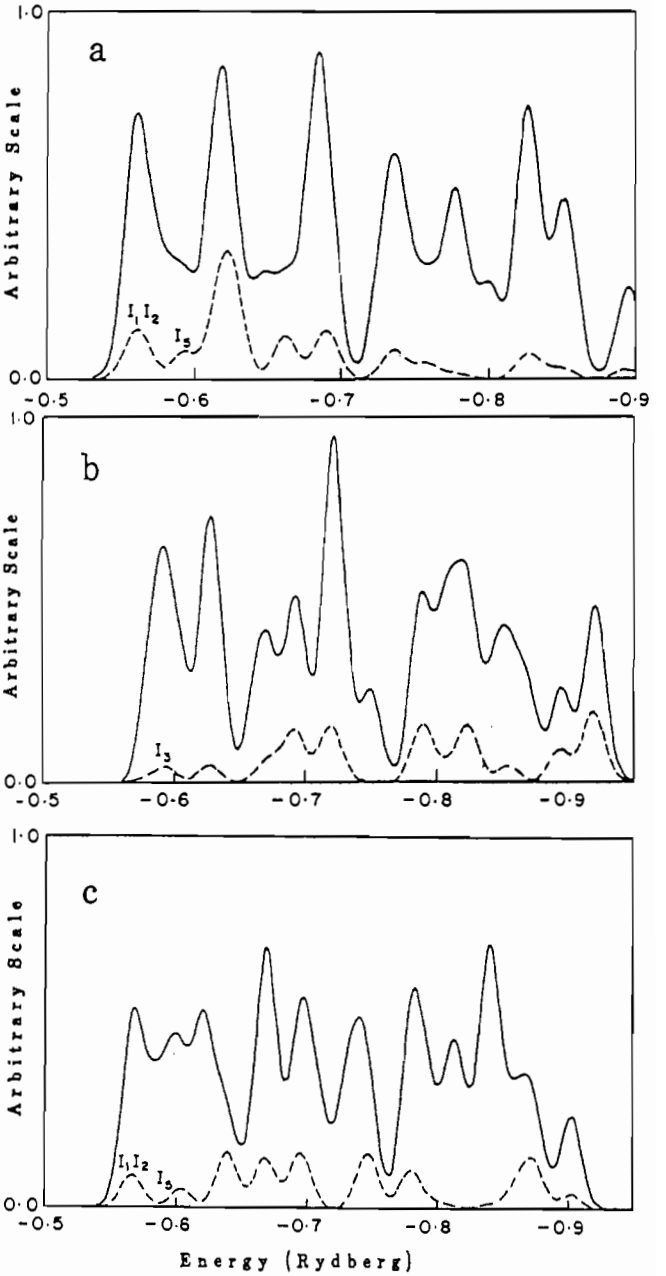

Figure 15. Convolutioin of the molecular orbital energies (solid line) and the convolution of the d component of the central metal (dashed line) for the thiomolybdate complex ions (a) $[Ni(MoS_4)_2]^{2-}$, (b) $[Pd(MoS_4)_2]^{2-}$, and (c) $[Pt(MoS_4)_2]^{2-}$.

does not seem to be any justificatioin, however, why such a splitting had not been observed in the Pt analogue.

The theoretical ionization energies were calculated by using the transition-state method of Slater.[37] These are summarized in Table XII, in which we report the ionization energies for the highest five occupied MO's for the series of complex ions under study. The ionization energies of the thiomolybdate complex ions are seen to be larger than the thiotungstate analogues. Perhaps the best approach to analyze the ionization energy is to convolute the respective orbital energies by using a Gaussian or Lorentzian distribution function. Using the former representation leads to an equation that takes the form

$$g(\epsilon) = \sum_i \frac{n_i q_i}{(2\pi\sigma)^2} \exp\left[\frac{-(\epsilon - \epsilon_i)^2}{2\sigma^2}\right] \qquad (14)$$

where n_i, q_i, and ϵ_i are the occupancy, charge, and the energy of the ith molecular orbitals, respectively, in which the broading parameter, σ, is set equal to 0.008. Similar convolutions of the d component of the central metal in respective molecular orbitals may be obtained. In Figure 15, we demonstrate these convolutions in the case of the thiomolybdate complex ions. In this figure, the convolution of the orbital energies premultiplied by a factor that represents the fraction of the charge carried by the central metal d bases (dashed line) is superposed on similar convolutions for the orbital energies (solid line). Ionization from the ith molecular

orbital is identified as I_1. In Figure 15a, we illustrate the convolution for the $[Ni(MoS_4)_2]^{2-}$ complex ion. Ionization from orbitals that have large contribution from the Ni d bases are identified in the figure as $I_1(5b_{2g})$, $I_2(3b_{3g})$, and $I_5(4b_{2g})$. Peaks $I_3(4b_{1u})$ and $I_4(2a_u)$ are not identified because they involve orbitals that have no contribution from the central metal d bases. In the case of the Pd complex ion, there is only one ionization peak that involves orbitals with appreciable Pd(d) bases and it is identified as $I_3(3b_{3g})$. The relative composition of the d component is seen to be much smaller than in the nickel analogue. In $[Pt(MoS_4)_2]^{2-}$ we identify three ionization peaks, namely I_1, I_2, and I_5 that are equivalent to the $[Ni(MoS_4)_2]^{2-}$ analogue but have a smaller contribution from the central metal d component. It is also apparent that the contribution of the d component in the higher occupied orbitals is much larger in the $[Ni(MoS_4)_2]^{2-}$ complex ion. The reverse is true for the lower occupied orbitals. It is only unfortunate that there is no experimental data regarding the ionization energies of these species that one can compare with and these values are included only for future validation. We point out, however, that $X\alpha$ binding energies are reported to be overestimated by ~20%. Binding energies of carbonyl to a single Pd atom or to a Pd dimer have been reported by Blomberg et al.[55] by employing a large basis set using the size-consistent coupled pair functional with CI. The chemisorption energy of CO on a Pd surface is determined by these authors to be much smaller than the binding energy to the dimer and is therefore consistent with relativistic $X\alpha$ calculations using the LCGTO-VWN model potential on the same system reported by Andzelm and Salahub.[56]

Acknowledgment. We express our gratitude to Professor Pekka Pyykkö of the Chemistry Department, University of Helsinki, Finland, for kindly reviewing this paper. Acknowledgmenet is also made to the Research Management Unit at Kuwait University for supporting this work (Project SC044).

Registry No. $[NiMo_2S_8]^{2-}$, 66616-04-4; $[PdMo_2S_8]^{2-}$, 71035-56-8; $[PtMo_2S_8]^{2-}$, 71035-58-0; $[NiW_2S_8]^{2-}$, 45845-07-6; $[PdW_2S_8]^{2-}$, 71035-57-9; $[PtW_2S_8]^{2-}$, 71035-59-1.

Supplementary Material Available: Tables IV-VIII listing molecular orbital energies and charge compositions of the MO's (5 pages). Ordering information is given on any current masthead page.

(55) Blomberg, M. R. A.; Lebrilla, C. B.; Siegbahn, E. M. *Chem. Phys. Lett.* **1988**, *150* (6), 522-528.
(56) Andzelm, J.; Salahub, D. R. *Int. J. Quantum Chem.* **1986**, *29*, 1091-1104.

Contribution from the Departamento de Química Inorgánica, Universidad de Murcia, 30071-Murcia, Spain, Departamento de Química, Universidad Autônoma de Barcelona, 08193-Bellaterra, Barcelona, Spain, and Instituto de Ciencia de Materiales CSIC, Martí y Franqués s/n, 08028 Barcelona, Spain

Synthesis, Structural Characterization, and Reactivity toward Weak, Protic Electrophiles of $[(C_6F_5)_2Pd(\mu\text{-}OH)_2Pd(C_6F_5)_2]^{2-}$

Gregorio López,*,† José Ruiz,† Gabriel García,† Consuelo Vicente,† Jaime Casabó,‡ Elíes Molins,§ and Carlos Miravitlles§

Received November 20, 1990

The bis(μ-hydroxo) complex $Q_2[(C_6F_5)_2Pd(\mu\text{-}OH)_2Pd(C_6F_5)_2]$ (**1**) (Q = NBu_4) has been obtained by reaction of *cis*-$Pd(C_6F_5)_2(PhCN)_2$ with 20% aqueous QOH in acetone. **1** reacts with weak, protic electrophiles H(LL) in the 1:2 molar ratio to give $Q_2[(C_6F_5)_2Pd(\mu\text{-}LL)_2Pd(C_6F_5)_2]$ [LL = pyrazolate (**2**), 3,5-dimethylpyrazolate (**3**), 3-methylpyrazolate (**4**), indazolate (**5**)]. The reaction between **1** and H(LL) (acetylacetone, benzoylacetone, 8-hydroxoquinoline) in acetone leads to the formation of the corresponding mononuclear complexes $Q[(C_6F_5)_2Pd(LL)]$ (**6-8**). $Q_2[(C_6F_5)_2Pd(\mu\text{-}OH)(\mu\text{-}dmpz)Pd(C_6F_5)_2]$ (**9**) has been produced by treatment of $Q_2[(C_6F_5)_2Pd(\mu\text{-}Cl)_2Pd(C_6F_5)_2]$ with QOH and Hdmpz (1:2:1 molar ratio) in methanol. IR and ^1H and ^{19}F NMR spectra have been used for structural assignments. An X-ray structural determination, carried out with $(NBu_4)_2[(C_6F_5)_2Pd(\mu\text{-}OH)_2Pd(C_6F_5)_2]$, has established the centrosymmetric binuclear nature of the anion, and the geometry around each Pd atom is that of a distorted planar square with Pd-O = 2.077 (6) and 2.068 (6) Å and Pd-C distances of 1.997 (7) and 2.006 (6) Å.

Introduction

The relative paucity of hydroxo complexes of the late transition metals has been attributed to the commonly believed reason that the M-OH bonds should be intrinsically weak owing to the mismatch of a hard, basic ligand (OH^-) with a soft metal center. The relatively recent work, however, suggests that the L_nM-OH bonds in hydroxo complexes are stronger than L_nM-C bonds in alkyl complexes.[1]

Synthetic routes used to prepare monomeric hydroxo complexes[1] of the nickel group elements include metal exchange,[2-4] oxidative addition,[5] and irreversible,[6] or reversible,[2a,b,3b,6d,7,8] σ-ligand metathesis reactions. Recently, some hydroxo-bridged complexes of nickel,[9a,b] palladium,[10] and platinum[10-12] have been described.

The recent surge of interest in the chemistry of hydroxo complexes of the nickel group elements is undoubtedly related to their interesting reactivity and potential relevance to catalysis.

On the other hand, in the reported $K_2[Pd(C_6F_5)_4]$-catalyzed cyclotrimerization of malononitrile,[13] the identity of the actual catalyst was left unexplored. The presence of a hydroxo-palladium species, generated in situ by hydrolysis of $[Pd(C_6F_5)_4]^{2-}$, could

† Universidad de Murcia.
‡ Universidad Autônoma de Barcelona.
§ Instituto de Ciencia de Materiales.

(1) Bryndza, H. E.; Tam, W. *Chem. Rev.* **1988**, *88*, 1163.
(2) (a) Ros, R.; Michelin, R. A.; Bataillard, R.; Roulet, R. *J. Organomet. Chem.* **1979**, *161*, 75. (b) Michelin, R. A.; Napoli, M.; Ros, R. *J. Organomet. Chem.* **1979**, *175*, 239. (c) Sinigalia, R.; Michelin, R. A.; Pinna, F.; Strukul, G. *Organometallics* **1987**, *6*, 728.
(3) (a) Appleton, T. G.; Bennett, M. A. *Inorg. Chem.* **1978**, *17*, 738. (b) Arnold, D. P.; Bennett, M. A. *J. Organomet. Chem.* **1980**, *199*, 119.
(4) (a) Villain, G.; Kalck, P.; Gaset, A. *Tetrahedron Lett.* **1980**, *21*, 2901. (b) Gaset, A.; Constant, G.; Kalck, P.; Villain, G. *J. Mol. Catal.* **1980**, *7*, 355.
(5) Yoshida, T.; Matsuda, T.; Okano, T.; Kitani, T.; Otsuka, S. *J. Am. Chem. Soc.* **1979**, *101*, 2027.
(6) (a) Bennett, M. A.; Roberston, G. B.; Whimp, P. O.; Yoshida, T. *J. Am. Chem. Soc.* **1973**, *95*, 3028. (b) Bennett, M. A.; Yoshida, T. *J. Am. Chem. Soc.* **1978**, *100*, 1750. (c) Bennett, M. A.; Rokicki, A. *Aust. J. Chem.* **1985**, *38*, 1307. (d) Bennett, M. A. *J. Organomet. Chem.* **1986**, *300*, 7.
(7) Yoshida, T.; Okano, T.; Otsuka, S. *J. Chem. Soc., Dalton Trans.* **1976**, 993.
(8) Bryndza, H. E.; Calabrese, J. C.; Wreford, S. S. *Organometallics* **1984**, *3*, 1603.
(9) (a) Carmona, E.; Marín, J. M.; Paneque, M.; Poveda, M. L. *Organometallics* **1987**, *6*, 1757. (b) Carmona, E.; Marín, J. M.; Palma, P.; Paneque, M.; Poveda, M. L. *Inorg. Chem.* **1989** *28*, 1985.

0020-1669/91/1330-2605$02.50/0